Biosensors and Bioelectronics 178 (2021) 113022

Contents lists available at ScienceDirect

Biosensors and Bioelectronics

journal homepage: http://www.elsevier.com/locate/bios

A ratiometric electrochemiluminescence strategy based on two-dimensional nanomaterial-nucleic acid interactions for biosensing and logic gates operation

Liping Zhu [a], Linying Yu [a,b], Jing Ye [a], Mengxia Yan [a,b], Yao Peng [a], Jianshe Huang [b,**], Xiurong Yang [a,b,*]

[a] Department of Chemistry, University of Science and Technology of China, Hefei, Anhui, 230026, PR China
[b] State Key Laboratory of Electroanalytical Chemistry, Changchun Institute of Applied Chemistry, Chinese Academy of Sciences, Changchun, Jilin, 130022, PR China

ARTICLE INFO

Keywords:
Electrochemiluminescence
Hybridization chain reaction
Resonance energy transfer
Ratiometric biosensor
Logic gates

ABSTRACT

Two-dimensional (2D) nanomaterial-nucleic acid interactions have been widely used in the construction of fluorescent sensors, but they are rarely used in the construction of electrochemiluminescent (ECL) sensors and have never been used in the design of ratiometric ECL sensors. Therefore, a ratiometric ECL sensing platform was developed in this study based on the ECL resonance energy transfer (ECL-RET) of graphitic carbon nitride nanosheets (GCNNs)/$Ru(bpy)_3^{2+}$ donor/acceptor pair. The 2D GCNNs showed much weaker affinity to the long dsDNA duplexes formed by hybridization chain reaction (HCR) than $Ru(bpy)_3^{2+}$-lableled fuel hairpin DNAs (H1 and H2) for HCR. Therefore, the target-initiated HCR resulted in the luminescence enhancement of the GCNNs at 460 nm and the luminescence attenuation of the $Ru(bpy)_3^{2+}$ at 610 nm. By measuring the $I_{460\ nm}/I_{610\ nm}$ ratios, quantitative analysis of microRNA-133a was realized with a limit of detection of 0.41 pM. In addition, this ECL-RET sensing platform can be easily extended to detect metal ions or aptamer substrates by simply redesigning helper DNAs without changing the sequences of fuel hairpin DNAs. Moreover, due to the programmability of HCR, a series of sensitive logic gates ("OR", "INHIBIT", "AND", "NAND" and "INHIBIT-OR") based on the ECL-RET ratiometry can be constructed and responded to as low as 100 pM of Hg^{2+} or Ag^{+}.

1. Introduction

Two-dimensional (2D) nanomaterials such as graphene, transition metal dichalcogenides (TMDs), 2D metal-organic frameworks (MOFs) and transition metal oxides (TMOs) have aroused great research interest due to their large specific surface areas, attractive electronic and chemical properties (Chen et al., 2015; Liu et al., 2019; Peng et al., 2017; Wu et al., 2021; Xiong et al., 2017). In particular, their excellent fluorescence quenching ability and significantly different affinity to single-stranded DNA (ssDNA) and double-stranded DNA (dsDNA) enabled the establishment of many interesting fluorescence sensing platforms based on 2D nanomaterial-nucleic acid interactions (Huang et al., 2014; Liu et al., 2015; Tan et al., 2015; Zhu et al., 2017). For example, dyes/nanoclusters-labeled ssDNA/aptamer can be strongly adsorbed on the surface of 2D nanomaterials via π-π stacking, resulting in the fluorescent quenching (Liu et al., 2019; Wang et al., 2019). However, when the complementary DNA strands or aptamer substrates are present, the formed dsDNA duplexes or aptamer-substrate complexes exhibit much weaker adhesion and desorb from the 2D nanomaterials surface. As a result, the fluorescence of dyes or nanoclusters are recovered. Considering that the single signal output mode is susceptible to complex reaction environment, some novel fluorescence resonance energy transfer (FRET)-based ratiometric strategies have been developed through the combination of 2D nanomaterials with nucleic acid molecules (Mo et al., 2017; Yuan et al., 2019; Zhu et al., 2015). Thus, the accuracy and repeatability of the sensing systems are greatly improved.

Although, based on 2D nanomaterial-nucleic acid interactions, many remarkable progresses and achievements have been made in biosensing applications, they are mainly concentrated in the field of fluorescence sensing. The application of nucleic acid-functionalized 2D nanomaterials in electrochemiluminescence (ECL) assays remains largely

* Corresponding author. Department of Chemistry, University of Science and Technology of China, Hefei, Anhui, 230026, PR China.
** Corresponding author.
E-mail addresses: huangjs@ciac.ac.cn (J. Huang), xryang@ciac.ac.cn (X. Yang).

https://doi.org/10.1016/j.bios.2021.113022
Received 3 January 2021; Received in revised form 18 January 2021; Accepted 18 January 2021
Available online 21 January 2021

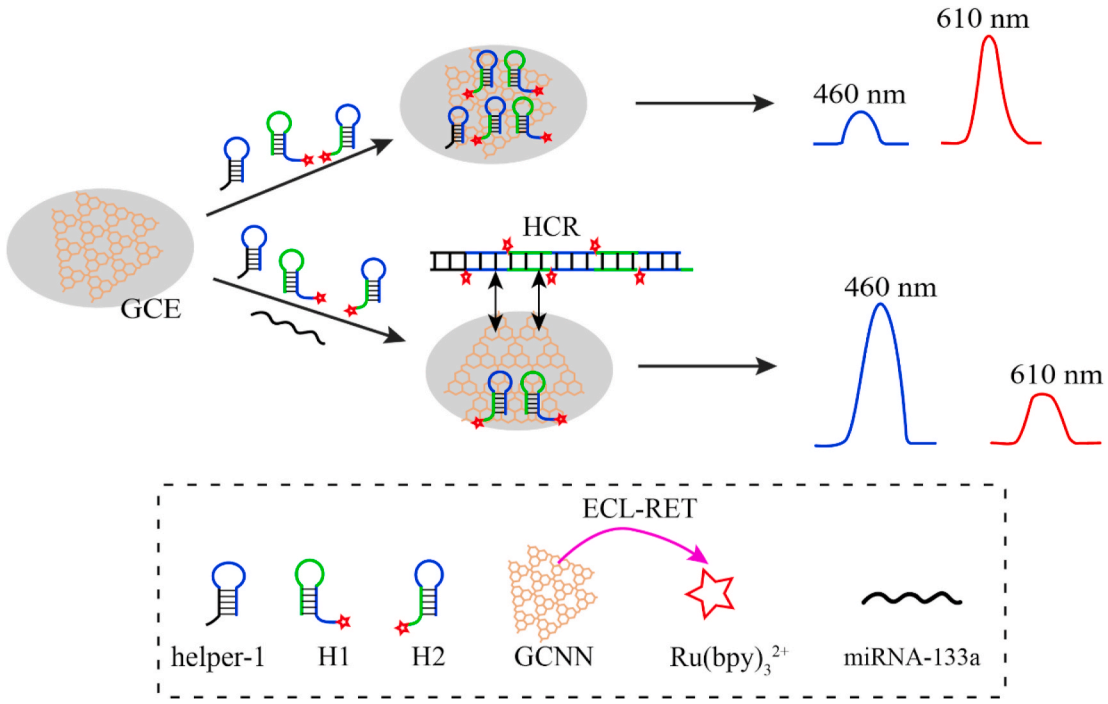

Scheme 1. Schematic illustration of 2D GCNNs-nucleic acid interactions-based ECL-RET ratiometry.

unexplored (Feng et al., 2015) and, to our knowledge, has never been reported for constructing ratiometric ECL resonance energy transfer (ECL-RET) biosensors. Compared with fluorescence sensing, ECL sensors exhibit a near-zero background since no excitation light source is required (Lv et al., 2020; Richter, 2004; Zhai et al., 2017). Accordingly, we can speculate that ratiometric ECL-RET platform, established with

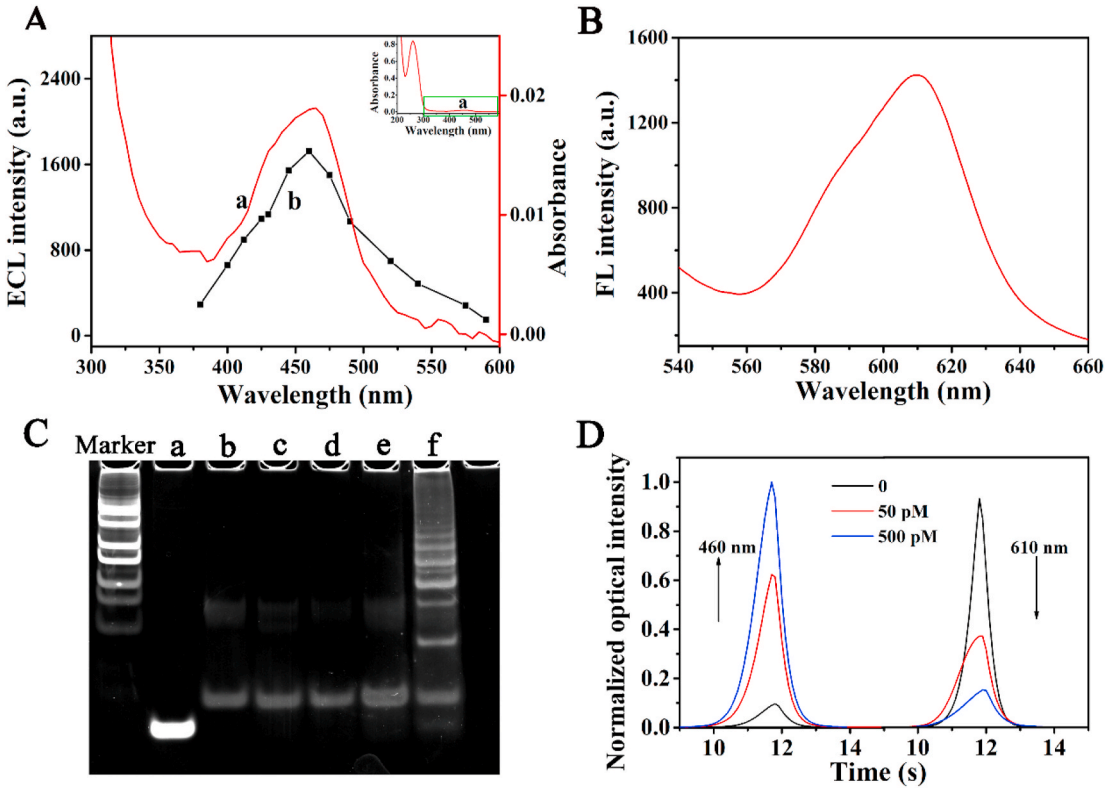

Fig. 1. (A) UV–vis absorption spectrum of $Ru(bpy)_3^{2+}$ modified on hairpin DNA (a) and the ECL spectrum of the GCNNs modified GCE (b). The inset shows the UV–vis absorption spectrum of $Ru(bpy)_3^{2+}$-H1/H2 in the range of 200–600 nm. The ECL spectrum was obtained through a series of optical filters with the blocking wavelength from 360 nm to 590 nm, and the photomultiplier tube (PMT) was set at 300 V. (B) Fluorescence spectrum of $Ru(bpy)_3^{2+}$ (λ_{ex} = 400 nm). (C) PAGE image of HCR: (a) target, (b) helper-1, (c) H1, (d) H2, (e) helper-1+H1+H2 and (f) target + helper-1+H1+H2. (D) Normalized optical responses of GCNNs and $Ru(bpy)_3^{2+}$ before and after adding target.

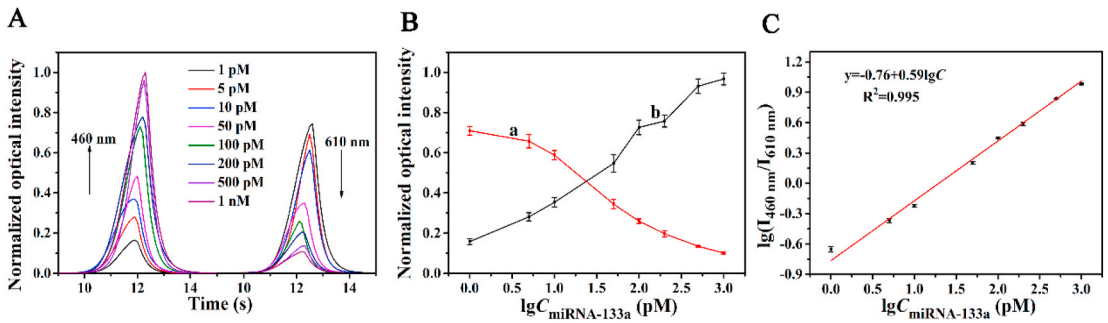

Fig. 2. (A) Normalized optical responses of GCNNs and $Ru(bpy)_3^{2+}$ at different miRNA-133a concentrations. (B) Relationship between the normalized optical intensity of (a) $Ru(bpy)_3^{2+}$ or (b) GCNNs and the logarithm of miRNA-133a concentration. (C) The calibration curve of $lg(I_{460\ nm}/I_{610nm})$ vs. $lgC_{miRNA\text{-}133a}$.

nucleic acid-functionalized 2D nanomaterials, can not only reserve the typical advantages of easy operation and high accuracy of FRET-based ratiometric sensors, but also can obtain higher sensitivity. Graphitic carbon nitride nanosheets (GCNNs), a graphene-like layered 2D nanomaterials, has good biocompatibility, efficient ECL emission and excellent luminescence stability (Liu et al., 2016; Xu et al., 2016; Zhou et al., 2018). These characteristics make it widely used in ECL sensing, especially the blue luminescence at 460 nm of GCNNs renders it a suitable candidate as energy donor for construction of ECL-RET biosensors (Feng et al., 2016; Zhu et al., 2019). Meanwhile, $Ru(bpy)_3^{2+}$ is frequently used as an energy acceptor to form acceptor/donor pair with GCNNs, which is attribute to its high fluorescence quantum yield and the perfect overlap between its absorption spectrum and ECL emission spectrum of GCNNs (Liang et al., 2018; Ye et al., 2019).

Based on the above considerations, an ECL-RET ratiometry based on the GCNNs/$Ru(bpy)_3^{2+}$ donor/acceptor pair was developed. Furthermore, in order to obtain better sensing performance, hybridization chain reaction (HCR), an isothermal enzyme-free amplification technique was used. As shown in Scheme 1, in the absence of target, helper hairpin DNA (helper-1), $Ru(bpy)_3^{2+}$-labeled fuel hairpin H1 and H2 remained in the hairpin state that were adsorbed on the surface of GCNNs. Hence, the ECL resonance energy transfer occurred between GCNNs and $Ru(bpy)_3^{2+}$. Due to the high RET efficiency from GCNNs to $Ru(bpy)_3^{2+}$ and high fluorescence quantum yield of $Ru(bpy)_3^{2+}$, the luminescence signal of the GCNNs at about 460 nm was almost completely quenched and the strong luminescence signal of the $Ru(bpy)_3^{2+}$ at about 610 nm was obtained. When the target was present, it opened helper-1, thus exposing the trigger strand to trigger the HCR. The produced H1/H2-based long dsDNA duplexes detached from the GCNNs surface, resulting in the increase of the luminescence signal of the GCNNs and the decrease of the luminescence signal of the $Ru(bpy)_3^{2+}$. By recording the ratios of GCNNs luminescence intensity to $Ru(bpy)_3^{2+}$ luminescence intensity ($I_{460\ nm}/I_{610\ nm}$) at different target concentrations, quantitative analysis of target microRNA-133a (miRNA-133a), a candidate biomarker of acute myocardial infarction (AMI), can be achieved. The as-proposed strategy of nearly unmodified-electrode surface has the characteristics of simplicity and rapidness (Hou et al., 2018).

More significantly, the oligonucleotides for HCR can be flexibly regulated by encoding specific functional information in their base sequences, rendering this sensing strategy an ideal candidate for the construction of programmable and versatile ECL-RET biosensor. Therefore, this sensing platform can not only be used for the detection of nucleic acid molecules, but also can be widely used for the detection of aptamer substrates and some metal ions. Exhilaratingly, the flexible design of the DNA sequences also makes this ECL-RET sensing platform applicable to the construction of DNA logic systems. In this work, we successfully designed "AND", "OR", "INHIBIT", "NAND" logic gates and a more advanced concatenated logic circuits "INHIBIT-OR". To the best of our knowledge, this is the first time that the integration of 2D nanomaterial-nucleic acid interaction with ECL-RET was utilized to construct DNA molecular logic gates.

2. Results and discussion

2.1. Characterization of the 2D GCNNs-Nucleic acid interaction-based ratiometric ECL-RET biosensor

As shown in Figs. S1 and S2, transmission electron microscope (TEM) and atomic force microscope (AFM) images show that the GCNNs have a sheet-like structure with a thickness of less than 3 nm, indicating the ultrathin GCNNs were obtained. The ECL spectrum of the GCNNs with an emission peak at 460 nm (Fig. 1A, curve b) matched well with the absorption spectrum of the $Ru(bpy)_3^{2+}$ (Fig. 1A, curve a), which is the basis of constructing an ECL-RET ratiometry. In addition, $Ru(bpy)_3^{2+}$ emitted a strong fluorescence with an emission peak of about 610 nm when excited at 400 nm (Fig. 1B). To verify the rationality of HCR design, native polyacrylamide gel electrophoresis (PAGE) experiments were carried out. As shown in Fig. 1C, in the absence of miRNA-133a, helper-1, H1 and H2 in the mixture maintained their respective stable hairpin structures (lane e). When the miRNA-133a was present, a series of bright stripes appeared (lane f), indicating the successful implementation of the target-initiated HCR. Fig. 1D shows the optical responses of GCNNs and $Ru(bpy)_3^{2+}$ before and after adding target miRNA-133a. In the absence of the target, helper-1, $Ru(bpy)_3^{2+}$-labeled H1 and H2 were adsorbed on the surface of GCNNs-modified glassy carbon electrode (GCE), the ECL of GCNNs was efficiently absorbed by the $Ru(bpy)_3^{2+}$ molecules, then the $Ru(bpy)_3^{2+}$ molecules were stimulated to emit light at 610 nm. After adding the target, the HCR reaction was triggered to generate long dsDNAs, which had good rigid structure and weak interaction force with GCNNs, resulting in a decrease in the amount of $Ru(bpy)_3^{2+}$ modified hairpin DNAs adsorbed on GCNNs. Therefore, the ECL of the GCNNs recovered to some extent, while the luminescence of $Ru(bpy)_3^{2+}$ reduced. Moreover, as the number of targets increased, the number of long dsDNA produced by HCR increased, the luminescence of 460 nm was further enhanced, and that of 610 nm was further reduced. The optical intensity of both wavelengths depended on the concentration of the target, which indicated the feasibility of ECL-RET ratiometry construction.

2.2. Analytical performance

Under the optimized conditions: 60 mM KCl in the TMK buffer (0.01 M Tris-HCl solution (pH 7.4), 5 mM $MgCl_2$), 90 min for HCR, pH 7.4 for optical signal detection solution as well as 0.30 μM of H1 and H2 (Fig. S3), the detection performance of the constructed ECL-RET ratiometry for miRNA-133a is shown in Fig. 2. With the increase of target concentration from 1 pM to 1 nM, the optical intensity at 460 nm tended to increase while that at 610 nm tended to decrease (Fig. 2A and B). Moreover, the logarithm of the ratio of the luminescence intensity at two wavelengths ($lg(I_{460\ nm}/I_{610\ nm})$) had a good linear correlation with the

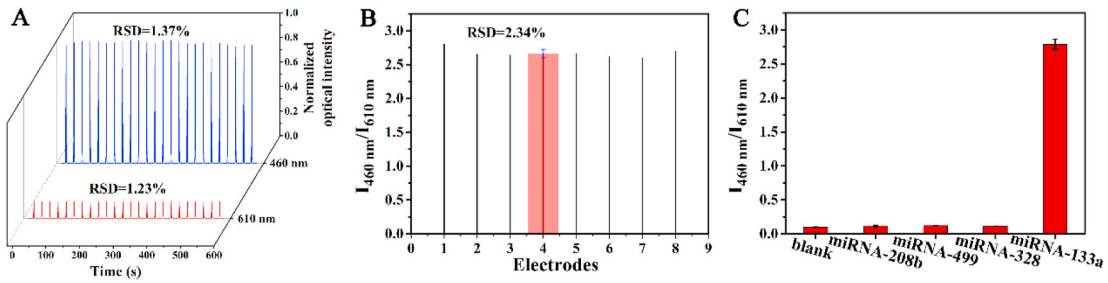

Fig. 3. (A) Normalized optical responses of the ECL-RET ratiometry under the continuous scanning of 24 cycles, the concentration of miRNA-133a was 500 pM. (B) The constructed ratiometric system was used to detect 100 pM miRNA-133a with 8 electrodes. (C) Selectivity analysis of the ECL-RET ratiometry, the concentration of miRNA-133a and other three interfering miRNAs was 100 pM.

logarithm of the miRNA-133a concentration with R^2 of 0.995 (Fig. 2C). The limit of detection (LOD) for miRNA-133a was 0.41 pM (S/N = 3), which is better than the fluorescence miRNA/DNA sensors based on 2D nanomaterial-nucleic acid interactions (Table S2), indicating that the ECL method combined with the 2D nanomaterial-nucleic acid interactions can indeed achieve higher sensitivity.

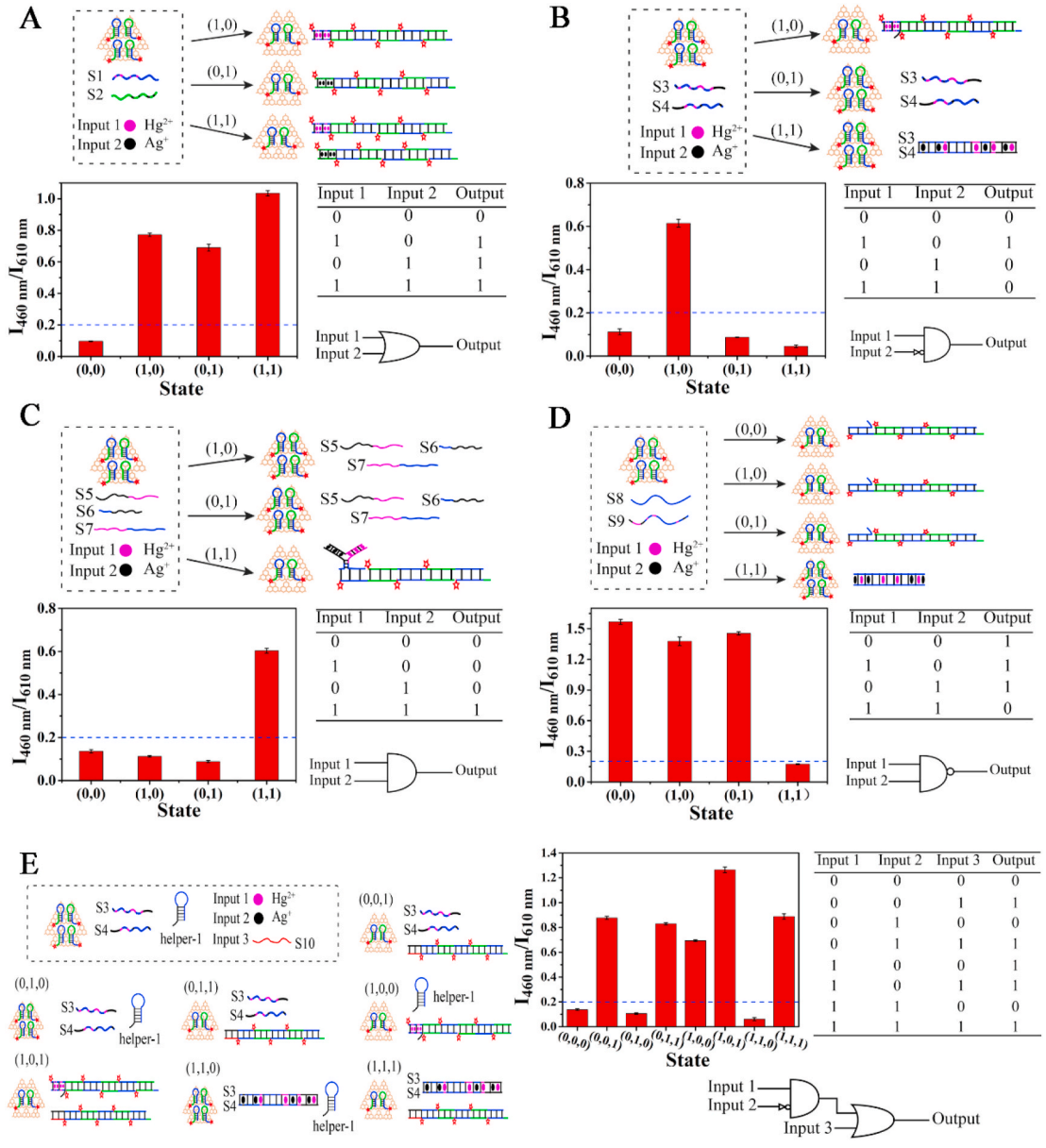

Fig. 4. The schematic illustration, $I_{460\ nm}/I_{610nm}$ response, truth table and electronic equivalent circuitry of "OR" logic gate (A), "INHIBIT" logic gate (B), "AND" logic gate (C), "NAND" logic gate (D) and "INHIBIT-OR" logic gate (E).

2.3. Stability, reproducibility and specificity of the ECL-RET ratiometry and its application in real sample analysis

The investigation of the stability of the ECL-RET ratiometry is shown in Fig. 3A. Under the continuous scanning of 24 cycles, the relative standard deviation (RSD) of optical signals at 460 nm was 1.37%, and that at 610 nm was 1.23%, indicating the excellent stability of the ratiometric system. As shown in Fig. 3B, the repeatability of the ratiometry was studied by detecting 100 pM of the miRNA-133a using eight electrodes, the RSD of $I_{460\ nm}/I_{610\ nm}$ ratios was 2.34%, showing that the ratiometric sensor with the dual signal output mode has a good repeatability. The specificity of the developed ratiometry was explored by using three miRNAs that are also related to the AMI as the interferers. The results are shown in Fig. 3C, the $I_{460\ nm}/I_{610\ nm}$ ratios of the three interferers were similar to that of blank sample and significantly different from that of miRNA-133a, demonstrating a good selectivity of the system. In addition, we investigated the practical application of the system by implementing the standard addition experiments in blank human serum samples. As shown in Table S3, acceptable recoveries of 104.20%–109.19% were obtained with RSD of 1.27%–3.12%, showing the potential of the ECL-RET ratiometry in clinical application.

2.4. The programmable targets detection

Due to the flexible regulation in DNA sequence, in addition to detecting the miRNA-133a, the ECL-RET ratiometry based on 2D GCNNs-nucleic acid interactions also has the potential to detect metal ions or aptamer substrates programmatically. As shown in Fig. S5, to verify this, we designed a helper ssDNA rich in thymine (helper-Hg^{2+}) and a helper hairpin DNA containing ATP aptamer (helper-ATP) for the detection of Hg^{2+} and ATP, respectively (the sequences of helper-Hg^{2+} and helper-ATP are shown in Table S1). In theory, when Hg^{2+} is present, helper-Hg^{2+} can bind with the toehold of helper-1 through T-Hg^{2+}-T coordination chemistry and open the hairpin structure, thus exposing the initiating chain and triggering the HCR (Fig. S5A). For ATP, its aptamer sequence was introduced into the loop of helper-ATP. In the presence of ATP, the hairpin structure is opened, also triggering the HCR (Fig. S5B). The actual experimental results of the optical signals at the two wavelengths after adding different Hg^{2+} or ATP concentrations are also shown in Fig. S5. The variation trend of luminescence intensity at both wavelengths presented the expected Hg^{2+} (Fig. S5A) or ATP (Fig. S5B) concentration dependence, confirming the possibility of programmable metal ions or aptamer substrates detection by the ECL-RET sensing platform.

2.5. Construction of logic gates

As indicated above, without changing the sequences of fuel hairpin DNAs (H1 and H2) for HCR, this programmable target detection platform can be easily extended to detect different targets by simply redesigning helper ssDNAs. Similarly, without changing the H1, H2 and the input targets (Hg^{2+} and Ag^{+} were used as target inputs of this study), just by simply redesigning helper ssDNAs, a series of sensitive logic gates ("OR", "INHIBIT", "AND" and "NAND") base on the ECL-RET ratiometry can be constructed (Fig. 4A–D). With the help of helper-1, even a more advanced concatenated logic circuits "INHIBIT-OR" can be constructed to realize the logical responses to three input targets (Hg^{2+}, Ag^{+} and ssDNAs S10) (Fig. 4E). In the following study of logic gates, the presence and absence of the targets were assigned as the inputs of 1 and 0, respectively.

As shown in Fig. 4A, two helper ssDNAs S1 and S2 were involved in the "OR" logic gate. S1 can bind with the toehold of H1 by the artificial T-Hg^{2+}-T bridges and open the hairpin structure of H1 to trigger the HCR. While S2 can hybridize with H2 by the artificial C–Ag^{+}-C bridges to trigger the HCR. The result of triggering HCR was the reduction of Ru$(bpy)_3^{2+}$-tagged H1 and H2 on the surface of the GCNNs, resulting in the increase of the luminescence of the GCNNs and the decrease of the luminescence of the Ru$(bpy)_3^{2+}$. The ratio of $I_{460\ nm}/I_{610\ nm}$ was recorded, a ratio of 0.2 was set as the threshold value. If the $I_{460\ nm}/I_{610\ nm}$ ratio was lower than 0.2, it would be regarded as the background signal and be defined as "0" output. When HCR occurred in the system, a high $I_{460\ nm}/I_{610\ nm}$ ratio greater than 0.2 was obtained and defined as "1" output. The $I_{460\ nm}/I_{610\ nm}$ ratios under various states in the "OR" logic gate, the corresponding truth table and the electronic equivalent circuitry are shown in Fig. 4A.

Similarly, two helper ssDNAs S3 and S4 were used in the "INHIBIT" logic gate. As shown in Fig. 4B, when Hg^{2+} was solely added, in other words, the input state was (1, 0), S3 can hybridize with H1 starting at the hairpin toehold via T-Hg^{2+}-T coordination chemistry, which triggered the HCR and obtained a high $I_{460\ nm}/I_{610\ nm}$ ratio to output "1". When Ag^{+} was added to the system alone, the hairpin structure of H1 and H2 cannot be opened. Subsequently, no HCR occurred and the output was "0". In the presence of Hg^{2+} and Ag^{+} at the same time, with the help of T-Hg^{2+}-T and C–Ag^{+}-C bridges, S3 and S4 can form six more consecutive complementary base pairs than S3 and H1. Therefore, in the input state of (1, 1), S3 was preferred to bind with S4 to form the stable S3–S4 duplex, the "0" output then would be obtained. As expected, the output was "1" only when Hg^{2+} was input separately, which was consistent with the proper operation of the "INHIBIT" logic gate.

As shown in Fig. 4C, the triggering sequence of the HCR was split into two domains, one was encoded at the 5′-end of S6, the other was encoded at the 3′-end of S7. With the help of T-Hg^{2+}-T and C–Ag^{+}-C bridges, the 5′- and 3′-end of ssDNA S5 hybridized with the 3′-end of S6 and the 5′-end of S7, respectively, to form the Y-shaped S6–S5–S7 structure. The formed S6–S5–S7 structure brought the two domains into close proximity to form an intact triggering sequence, which opened the hairpin structure of H1, resulting in the output of "1". In the other single input states, no S6–S5–S7 complex would be formed, the H1 and H2 would maintain the stable hairpin structure. Therefore, the $I_{460\ nm}/I_{610\ nm}$ ratios were lower than 0.2 and the outputs were "0". The $I_{460\ nm}/I_{610\ nm}$ responses of the "AND" logic gate in different states, the truth table and its electronic equivalent circuitry are shown in Fig. 4C.

The outputs of the "NAND" logic gate are "1" in all input states except the state of (1,1). Hence, two helper ssDNA S8 and S9 were designed to construct the logic gate (Fig. 4D). S8 can act as the trigger chain for the HCR to bind directly with H1 via the Watson-Crick base pairing principle and open the hairpin structure. S9 can hybridize with S8 completely through T-Hg^{2+}-T and C–Ag^{+}-C bridges to form stable S8–S9 duplex. Furthermore, there were more consecutive complementary base pairs in the S8–S9 duplex (28 base pairs) than in the S8–H1 complex (22 base pairs). Therefore, in the case of no input or single input states, S8 can trigger the HCR with outputs of "1". In contrast, when the input state was (1,1), S8–S9 duplex was formed preferentially, resulting in a low $I_{460\ nm}/I_{610nm}$ ratio, the output "0" was then obtained.

Moreover, a combinatorial "INHIBIT-OR" logic gate can be constructed by introducing a single strand of DNA (S10) as input 3 and the helper hairpin DNA (helper-1) into the "INHIBIT" logic gate. As shown in Fig. 4E, when S10 was present, it hybridized with the helper-1 and opened the hairpin structure. The opened helper-1 exposed the initiating chain sequence (the blue line), which can bind with H1 to trigger HCR resulting in the output of "1". When the input states were (0,0,1), (0,1,1), (1,0,0), (1,0,1) and (1,0,0), the $I_{460\ nm}/I_{610nm}$ responses were higher than the threshold value, the outputs were "1", otherwise the outputs were "0" for other inputs. In addition, by comparing states of (0,0,1) and (0,1,1), it was found that in the same case, the presence of Ag^{+} caused a slight decrease in the output signal (Fig. 4E). The reason may be that a small amount of Ag^{+} may be adsorbed on the GCNNs and occurs electron transfer with GCNNs, which slightly quenched the luminescence of GCNNs(Cao et al., 2018; Tang et al., 2013). This combinatorial gate can realize logic gate sensing for three targets and the targets could be of different kinds, indicating its huge potential of sensing application, especially for the multiplex sensing application.

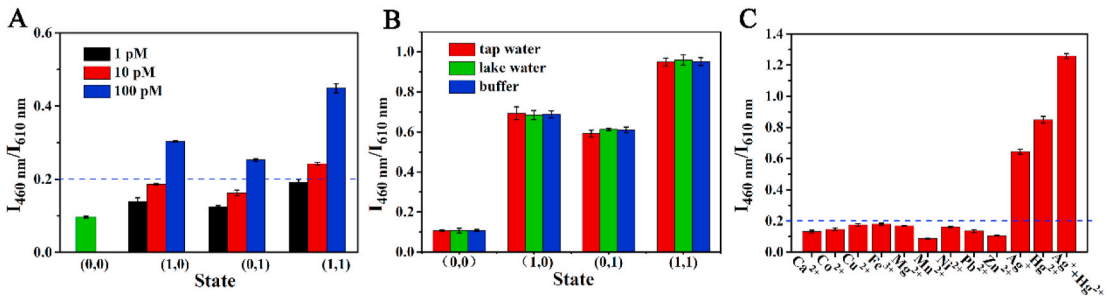

Fig. 5. Investigation of the sensitivity (A), practical application (B) and selectivity (C) of logic gates ("OR" gate as an example). The concentration of Hg^{2+} and Ag^{+} in B was 1 nM. The concentration of Hg^{2+}, Ag^{+} and all interfering metal ions in C was 2.5 nM.

2.6. Sensitivity, practicability and specificity of logic gates

As shown in Fig. 5, we selected "OR" gate as an example to examine the sensitivity, practicality, and specificity of the constructed logic gates. In the above constructed logic gates, the concentration of Hg^{2+} and Ag^{+} was 1 nM, well, what is the minimum input concentration at which the logic gates that can produce an expected feedback signal? We still took 0.2 as the threshold value and reduced the input concentration from 100 pM to 1 pM to study the sensitivity of the logic gates. In the "OR" gate, any single input or dual inputs, the outputs are "1". The experimental results in Fig. 5A show that when the input concentration was 100 pM, the operation results of the logic gate were consistent with the theory. When the input concentration continued to decrease, the response results were inconsistent with the truth table, indicating that the minimum input concentration at which the logic gate can produce the expected response was approximately 100 pM. As shown in Fig. 5B, to investigate the practicability of the logic gates, 1 nM Hg^{2+} or/and Ag^{+} were spiked into tap water, lake water and TNMK buffer (0.01 M Tris-HNO_3 solution (pH 7.4), 5 mM $Mg(NO_3)_2$ and 60 mM KNO_3) and "OR" gates were executed in the three water samples respectively. The response results of the logic gate in the three water samples showed no significant difference, indicating the potential application of logic gates in actual water samples. The investigation of the specificity for "OR" gate was shown in Fig. 5C, the logic gate showed significantly different responses to Hg^{2+} or/and Ag^{+} metal ions compared with other interfering metal ions, indicating excellent selectivity of the logic gate.

3. Conclusion

In summary, a ratiometric ECL-RET sensing platform based on 2D GCNNs-nucleic acid interactions was constructed in this study. In this ECL-RET ratiometry, the 2D GCNNs was used as energy donor and Ru $(bpy)_3^{2+}$ was the energy acceptor. Due to the conspicuous spectral overlap between the ECL emission spectrum of GCNNs and the absorption spectrum of Ru$(bpy)_3^{2+}$, the ratiometric sensor had high resonance energy transfer efficiency. The assembly of the sensing platform based on the significantly different affinity of GCNNs to hairpin DNAs and the HCR products (long dsDNA duplex) avoided the complex and tedious modification process of the electrode. Moreover, the signal amplification and programmability features of HCR made the ratiometric ECL-RET sensing platform be applicable not only to the sensitive detection of nucleic acid molecules, but also to the detection of aptamer substrates and some metal ions. Furthermore, benefiting from the versatility of the sensing platform, a series of sensitive logic gates ("OR", "INHIBIT", "AND", "NAND" and "INHIBIT-OR") were constructed with good specificity. The high sensitivity, flexible operations and the applicability in real samples analysis make the constructed ECL-RET ratiometry and logic gates as a promising platform for applications in disease diagnosis and DNA computing.

CRediT authorship contribution statement

Liping Zhu: Conceptualization, Data curation, Investigation, Methodology, Writing - original draft. **Linying Yu:** Investigation, Methodology, Resources, Writing - review & editing. **Jing Ye:** Resources. **Mengxia Yan:** Resources. **Yao Peng:** Resources. **Jianshe Huang:** Supervision, Writing - review & editing. **Xiurong Yang:** Funding acquisition, Project administration, Resources.

Declaration of competing interest

The authors declare no competing financial interest.

Acknowledgements

This work was supported by the National Natural Science Foundation of China (Nos. 22034006, 21627808 and 21721003), the Key Research Program of Frontier Sciences, CAS(QYZDY-SSW-SLH019), and the National Key Research and Development Program of China (2016YFA0201301).

Appendix A. Supplementary data

Supplementary data to this article can be found online at https://doi.org/10.1016/j.bios.2021.113022.

References

Cao, S., Chen, H., Jiang, F., Hu, Z., Wang, X., 2018. ACS Appl. Mater. Interfaces 10, 44624–44633.
Chen, Y., Tan, C., Zhang, H., Wang, L., 2015. Chem. Soc. Rev. 44, 2681–2701.
Feng, Q.M., Shen, Y.Z., Li, M.X., Zhang, Z.L., Zhao, W., Xu, J.J., Chen, H.Y., 2016. Anal. Chem. 88, 937–944.
Feng, Y., Wang, Q., Lei, J., Ju, H., 2015. Biosens. Bioelectron. 73, 7–12.
Hou, T., Xu, N., Wang, W., Ge, L., Li, F., 2018. Anal. Chem. 90, 9591–9597.
Huang, J., Gao, X., Jia, J., Kim, J.K., Li, Z., 2014. Anal. Chem. 86, 3209–3215.
Liang, R.P., Yu, L.D., Tong, Y.J., Wen, S.H., Cao, S.P., Qiu, J.D., 2018. Chem. Commun. 54, 14001–14004.
Liu, J., Wang, H., Antonietti, M., 2016. Chem. Soc. Rev. 45, 2308–2326.
Liu, M., Zhang, W.Q., Chang, D.R., Zhang, Q., Brennan, J.D., Li, Y.F., 2015. Trac. Trends Anal. Chem. 74, 120–129.
Liu, X., Zhang, H., Song, Z., Guo, L., Fu, F., Wu, Y., 2019. Biosens. Bioelectron. 129, 118–123.
Lv, W., Yang, Q., Li, Q., Li, H., Li, F., 2020. Anal. Chem. 92, 11747–11754.
Mo, L., Li, J., Liu, Q., Qiu, L., Tan, W., 2017. Biosens. Bioelectron. 89, 201–211.
Peng, Y., Huang, Y., Zhu, Y., Chen, B., Wang, L., Lai, Z., Zhang, Z., Zhao, M., Tan, C., Yang, N., Shao, F., Han, Y., Zhang, H., 2017. J. Am. Chem. Soc. 139, 8698–8704.
Richter, M.M., 2004. Chem. Rev. 104, 3003–3036.
Tan, C., Yu, P., Hu, Y., Chen, J., Huang, Y., Cai, Y., Luo, Z., Li, B., Lu, Q., Wang, L., Liu, Z., Zhang, H., 2015. J. Am. Chem. Soc. 137, 10430–10436.
Tang, Y., Song, H., Su, Y., Lv, Y., 2013. Anal. Chem. 85, 11876–11884.
Wang, Y., Wu, N., Guo, F., Gao, R., Yang, T., Wang, J., 2019. J. Mater. Chem. B 7, 7566–7573.
Wu, J., Lv, W., Yang, Q., Li, H., Li, F., 2021. Biosens. Bioelectron. 171, 112707.
Xiong, M., Rong, Q., Meng, H.M., Zhang, X.B., 2017. Biosens. Bioelectron. 89, 212–223.
Xu, H.F., Zhu, X., Dong, Y.Q., Wu, H.S., Chen, Y.M., Chi, Y.W., 2016. Sens. Actuators, B 236, 8–15.
Ye, J., Zhu, L., Yan, M., Zhu, Q., Lu, Q., Huang, J., Cui, H., Yang, X., 2019. Anal. Chem. 91, 1524–1531.

Yuan, D., Kong, J., Fang, X., Chen, Q., 2019. Talanta 196, 64–70.
Zhai, Q.F., Li, J., Wang, E.K., 2017. Chemelectrochem 4, 1639–1650.
Zhou, Z., Zhang, Y., Shen, Y., Liu, S., Zhang, Y., 2018. Chem. Soc. Rev. 47, 2298–2321.
Zhu, C., Du, D., Lin, Y., 2017. Biosens. Bioelectron. 89, 43–55.
Zhu, C.Z., Dan, D., Lin, Y.H., 2015. 2D Mater. 2.
Zhu, L., Ye, J., Yan, M., Zhu, Q., Yang, X., 2019. Analyst 144, 6554–6560.